A Study on the Improvement of Torque Density of an Axial Slot-Less Flux Permanent Magnet Synchronous Motor for Collaborative Robot

Dong-Youn Shin [1], Min-Jae Jung [2], Kang-Been Lee [3], Ki-Doek Lee [1] and Won-Ho Kim [2],*

[1] Intelligent Mechatronics Research Center, Korea Electronics Technology Institute, Seongnam-si 13509, Gyeonggi-do, Korea; tlsehddbs147@keti.re.kr (D.-Y.S.); kdlee@keti.re.kr (K.-D.L.)
[2] Department of Electrical Engineering, Gachon University, Seongnam-si 13120, Gyeonggi-do, Korea; wjdalswo12@naver.com
[3] Department of Electrical and Computer Engineering, Michigan State University, East Lansing, MI 48824, USA; leekangb@msu.edu
* Correspondence: wh15@gachon.ac.kr; Tel.: +82-31-750-5881

Abstract: In this paper, an axial slot-less permanent magnet synchronous motor (ASFPMSM) was designed to increase the power density. The iron core of the stator was replaced with block coils, and the stator back yoke was removed because 3D printing can provide a wide range of structures of the stator. The proposed model also significantly impacts efficiency because it can reduce iron loss. To meet size and performance requirements, coil thickness and number of winding layers in the block, the total amount of magnet, and pole/slot combinations were considered. The validity of the proposed model was proved via finite elements analysis (FEA).

Keywords: axial flux permanent magnet synchronous motor; SPMSM; slot-less; block-coil; collaborative robot (cobot); robot joint; 3D-print; Somaloy Core; torque density; output power density

1. Introduction

Many studies on radial flux permanent magnet synchronous motor (RFPMSM), applied in collaborative robots (cobots) and which can physically interact and share a workspace with humans, have been conducted [1–3]. However, the RFPMSM should be developed with consideration of material developments to meet high-performance requirements in industry because the performance and efficiency of the RFPMSM are saturated due to pioneer studies [4,5]. Furthermore, since there is an unfavorable structural problem of multi-joint motors applied in cobots, bilateral axial slot-less flux permanent magnet synchronous motor (ASFPMSM) with high power density has been addressed as a new motor model [6–8].

Theoretically, there is a limitation that it is hard to manufacture with a slot-less structure because the press die manufacturing method can provide only conventional structure [9]. Therefore, a new structure of the motor can be developed when the motor is manufactured using 3D printing technology with the core powder as Somaloy material. However, when the core powder is used, the B-H characteristics are lower than that of laminated electrical steel sheets, and iron loss, which influences the efficiency of the motor, is higher than that of laminated electrical steel sheets.

To compensate for the drawbacks of the 3D printing technology, a block coil, which can remove the slot of the stator where the coil is wound, and mold the coil with plastic, can be used to reduce iron loss. In addition, it is possible to reduce iron loss with a shape without the back yoke of the stator because of the closed magnetic flux loop made by facing the same permanent magnet poles during operation of the motor [10–13]. In addition, the output power and torque density of ASFPMSM manufactured by 3D printing can be higher

compared to RFPMSM [14–16]. In short, the advantages of eliminating the slot and the back yoke of the stator have a significant impact on the efficiency of the motor [17,18].

In this paper, improved output power density and torque density of an ASFPMSM applied in cobots were proposed via optimization design.

2. Target Model Specification

Among the permanent magnet synchronous motor types for collaborative robots, the radial flux type SPMSM (surface permanent magnet synchronous motors) motors are commonly used. Since the magnetic flux density distribution in the air gap is uniform in the SPMSM, the control is accurate. These advantages have a significant impact on minimizing the size of the motor. In addition, it is much easier to obtain more spaces for winding and weight reduction than in the case of the internal permanent magnet synchronous motor (IPMSM).

The general cobots used in a narrower working space should be considered their size requirements during machine design. Therefore, an optimization design process is required to maximize performance with limited requirements.

RFPMSM applied in actual cooperative robots was selected as the target model, as shown in Figure 1, to meet the performance and size requirements when a new model is designed.
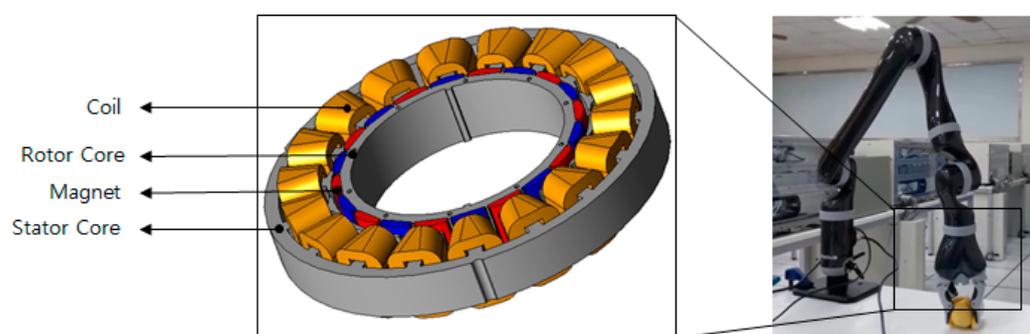
Figure 1. Radial Flux Permanent Magnet Synchronous Motor target model of cobots [1].

To ensure equal performance between the target model and an ASFPMSM, torque, no-load back EMF, and efficiency were considered. Based on the specifications, the ASFPMSM with 52.2 mm of outer rotor diameter was proposed with 0.55 Nm torque at 3500 rpm and 89.6% efficiency, as shown in Tables 1 and 2. The torque curve of the target model is presented in Figure 2. More detailed information related to the dimensions is presented later in the manuscript.

Table 1. The specifications of the target model.

Parameter	Value (mm)
Stator Outer Diameter	82
Stator Inner Diameter	54
Stator Teeth Width	3.3
Rotor Outer Diameter	52.2
Rotor Inner Diameter	44.8
Magnet Thickness	5
Air Gap	1
Stator Stack Length	10
Rotor Stack Length	13
Magnet Thickness	2

**Table 2.** Performance and materials of the target model.

	Parameter	Value	Unit
	Pole/Slot	20/18	-
	Rated Speed	3500	RPM
	Torque @3500 Rotating Per Minutes	0.55	Nm
	Current	5.1	A_{rms}
Performance	No-load L-L Back Electric Motive Force @3500 Rotating Per Minutes	26.28	V_{rms}
	Copper Loss	11.1	W
	Iron Core Loss	12.5	W
	Efficiency	89.6	%
	Direct Current Link	48	V
	Material	Copper	-
Winding	Diameter	0.85	mm
	Series Turns Per Phase	96	Turns
	Material	N42SH	-
Magnet	B_r	1.33	T
	H_c	1592	kA/m

Figure 2. Torque-Nominal Speed curve of the target model.

3. ASFPMSM Proposal Model Concept

3.1. Proposed ASFPMSM Concept

ASFPMSM applied in cobots should provide high output power density because their thin and small structures are needed to meet space limitations in cobots. Therefore, a new model of ASFPMSM is proposed in this paper. As mentioned above, since there are requirements related to size and power density in cobots, it is hard to meet the requirements with the existing winding method. A type of block coil using 3D printing technology can overcome the limitations. The block coil can be manufactured by molding the coil part with plastic using 3D printing technology, as shown in Figure 3. The winding part of the motor can be designed because the 3D printing technology provides the freedom to create the desired model, as shown in Figure 3a,b.
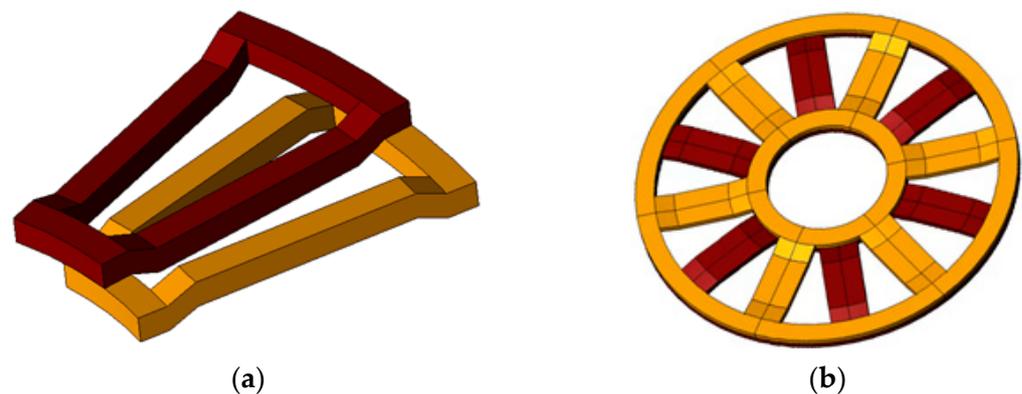
Figure 3. (**a**) Part where the coil is wound; (**b**) shape of assembling block coil.

Furthermore, when the rotor N and S poles are designed to face each other in both directions, the facing permanent magnet and the rotor back yoke form a closed loop of magnetic flux. This structure can eliminate the stator back yoke. Finally, multi-poles and multi-slot structure were selected to design a thin motor.

An amount of magnetic flux per pole, which influences the performance of the motor, can be presented as shown in Equation (1). This equation provides some facts that magnetic flux is proportional to the difference between the square of the inner diameter and the square of the outer diameter of the ASFPMSM. Furthermore, the magnetic flux per pole can be reduced as the number of poles increases. This correlation proved that the width of the back yoke of the rotor of ASFPMSM could be decreased as thin as possible when a big number of pole-slot combination is applied in the motor because the magnetic flux per pole can be reduced.

$$\Phi_f = \int_{R_{in}}^{R_{out}} a_i B_{mg} \frac{2\pi}{2p} r \, dr = a_i B_{mg} \frac{\pi}{2p} (R_{out}^2 - R_{in}^2) \tag{1}$$

3.2. Analysis of Proposed ASFPMSM

To make a comparative analysis based on the same criteria as the target model, the total laminated length of ASFPMSM was set to 13 mm. The rotor radius was adjusted according to the stator radius of RFPMSM, and the same winding specifications were designed. In addition, since the ASFPMSM does not have a stator shoe and teeth, the laminated length, excluding the air gap length (block coil height) and core back yoke thickness, is designed to be the same length as the magnet thickness to increase the back electromotive force (back EMF). The ASFPMSM is presented with the same laminated length and winding specifications as the target model in Figure 4a,b.
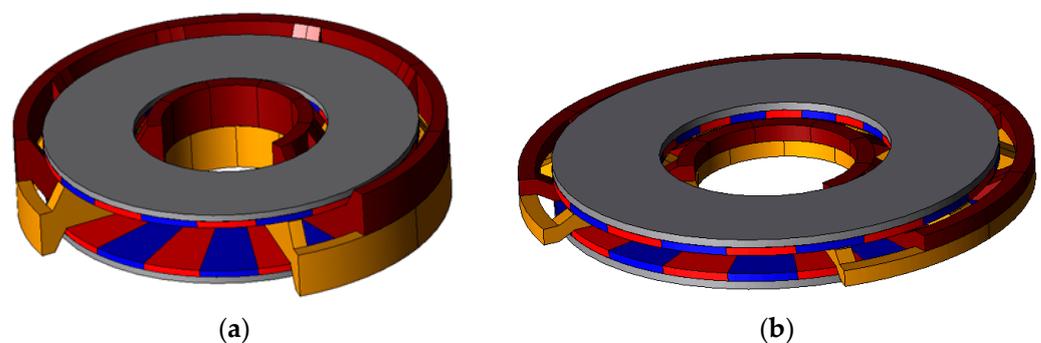
Figure 4. (**a**) Same laminated length model as the target model; (**b**) a same number of turns model as the target model.

A comparative analysis of the vector plot of the target model under no load and the proposed ASFPMSM model under no-load was performed at a rated speed of 3500 rpm, as shown in Figure 5.

(**a**)   (**b**)
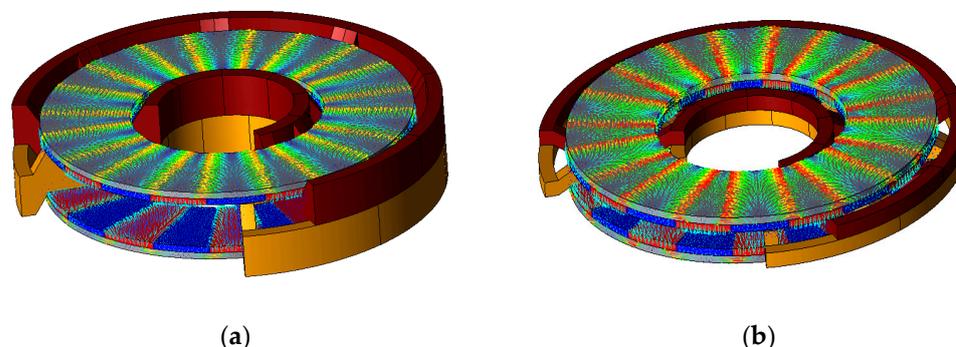
Figure 5. (**a**) Flux line in the same laminated length model as the target model, (**b**) flux line of the same turn number model as the target model.

The vector diagram confirmed that the low back EMF is due to the air gap length increasing as the coil height increases. The magnetic flux of the permanent magnet did not reach the back yoke of the stator and leaked to the next magnet. As a result, it is necessary to find the minimum air gap length for the magnetic flux to reach the back yoke of the stator and to make the magnetic flux closed-loop possible, and to design a design with the maximum number of turns within the air gap length while minimizing the use of magnets.

3.3. ASFPMSM Optimal Coil Height Analysis

In ASFPMSM, the airgap length value is increased by the height of the block coil because there are no stator teeth and shoes. Therefore, airgap length has a significant influence on the performance of the motor compared to other types of motors. Thus, flux paths were analyzed at various block coil heights (1~6 mm), respectively, to increase the performance, as shown in Figure 6.

In Figure 6, the coils are located in the empty space between the rotor and the stator, and the coils are molded with plastic material using 3D printing. Therefore, since the coil part becomes an air gap, after removing the coil part, the vector diagram of the magnetic flux was checked to make it easier to check the flow of the magnetic flux.

The results of analyzing the magnetic flux vector diagram for each coil height are as follows. When the block coil height is 1~2 mm, the leakage flux is minimized, and the magnetic flux path forms a closed loop with the back yoke of the stator. Models with a block coil height of 3 mm or more could not produce the desired performance due to large magnetic flux leakage, as shown in Figure 6. Therefore, since the winding height of the target model is 0.85 mm, a value between 1 mm and 2 mm, a height of 1.7 mm block coil, which is a multiple of 0.85 mm, was selected as the optimal height.

Since 0.85 mm is close to 1 mm, even though it is not within the optimal height range (1~2 mm), both 0.85 mm and 1.7 mm of the block coil height were selected for 1-layer winding and 2-layer winding to conduct accurate performance analysis, as shown in Figure 7a–d. Both models have their pros and cons. Although the 1-layer winding model has a short airgap length, when winding four turns per coil side, the number of serial turns is 24 turns, so it is difficult to expect a good performance. The 2-layer model has better performance because it can wind up to 48 turns, despite the longer airgap length compared to the 1-layer model. No-load back EMFs are presented to validate that the 2-layer model, which has 1.7 coil height, has a better performance compared to the 1-layer model, as shown in Figure 8. As a result, it was found that 1.7 mm is the most optimal value for coil height.
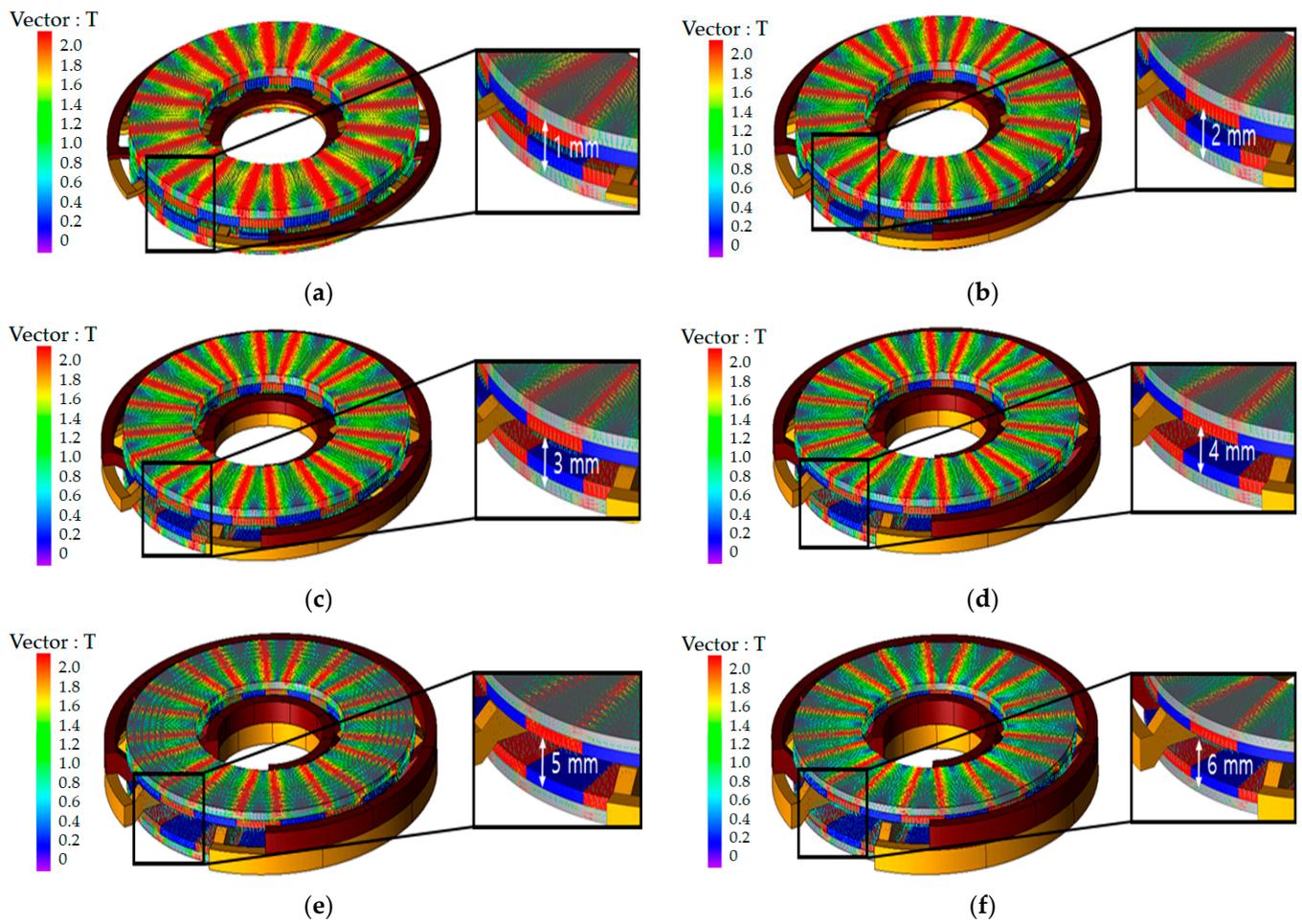
Figure 6. Flux line analysis according to block coil height. (**a**) Block-Coil Thickness 1 mm, (**b**) Block-Coil Thickness 2 mm, (**c**) Block-Coil Thickness 3 mm, (**d**) Block-Coil Thickness 4 mm, (**e**) Block-Coil Thickness 5 mm, (**f**) Block-Coil Thickness 6 mm.
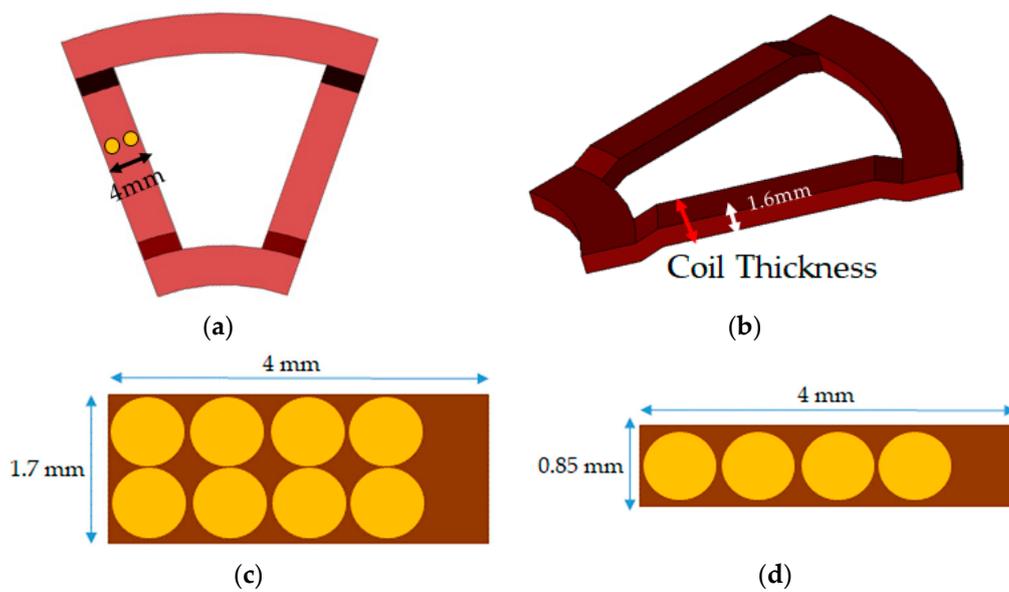

Figure 7. (**a**) Shape of coil width, (**b**) coil height, (**c**) coil area of coil height 1.7 mm, (**d**) coil area of coil height 0.85 mm.
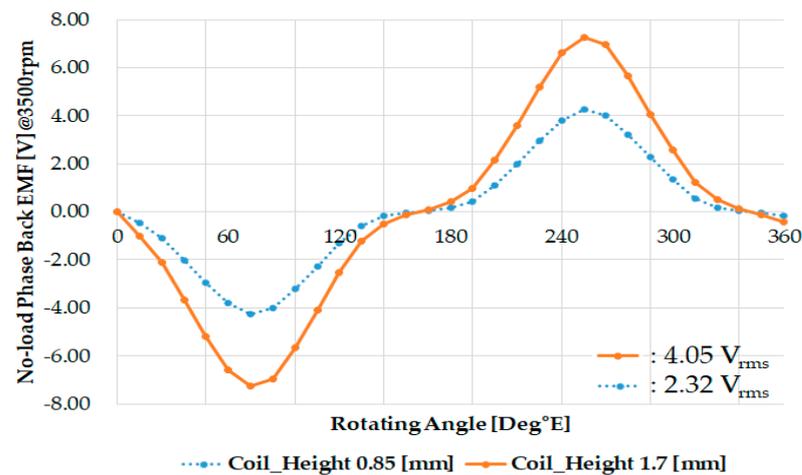
Figure 8. No load phase back-EMF compared to coil height 0.85 mm (Blue) and coil height 1.7 mm (Red).

### 3.4. ASFPMSM Optimal Magnet Size Analysis

In order to select a reasonable amount of magnet while minimizing leakage flux from the optimal block coil thickness analyzed previously, the performance analysis was conducted by changing the amount of magnet in the axial direction. Back EMFs were compared and analyzed between models with the total magnet thickness from 2 mm to 10 mm, as shown in Figure 9.

(a)   **(b)**
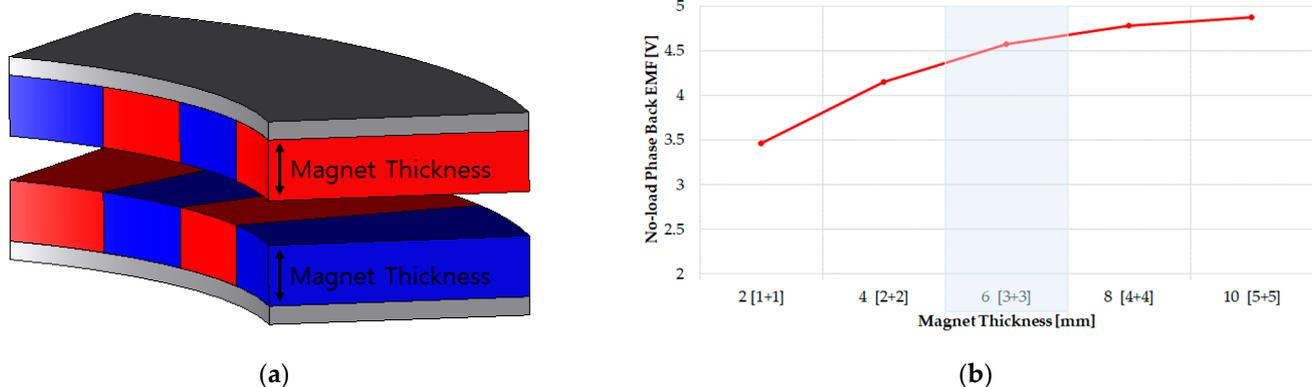
Figure 9. Analysis of no load phase back EMF according to magnet thickness. (**a**) Magnet Thickness, (**b**) No load phase Back EMF according to Magnet Thickness.

As a result of the analysis of no-load back EMF according to various amounts of magnet, it was confirmed that back EMF increases as magnet thickness increases until 6 mm. However, the performance was saturated when the total magnet thickness is larger than 6 mm. It is possible that back EMF does not increase because of saturation of the core. Therefore, whether no-load back EMF saturation is from core saturation or not should be checked from simulation results with various core thicknesses, as shown in Figure 10.

From the result presented in Figure 10, the fact that no-load back EMF does not increase as magnet thickness increases is not from the saturation of the core. There is a correlation between the core thickness and the total amount of magnet. Since the laminated length was fixed to 13 mm, after determining the thickness of the coil, the remaining laminated length is used as the core thickness and the magnet thickness. Therefore, the thinner the core, the greater the amount of magnet can be used. Considering that the stacking length of the target model is 13 mm, the optimal core thickness was selected as 2 mm to minimize the size of the proposed motor.
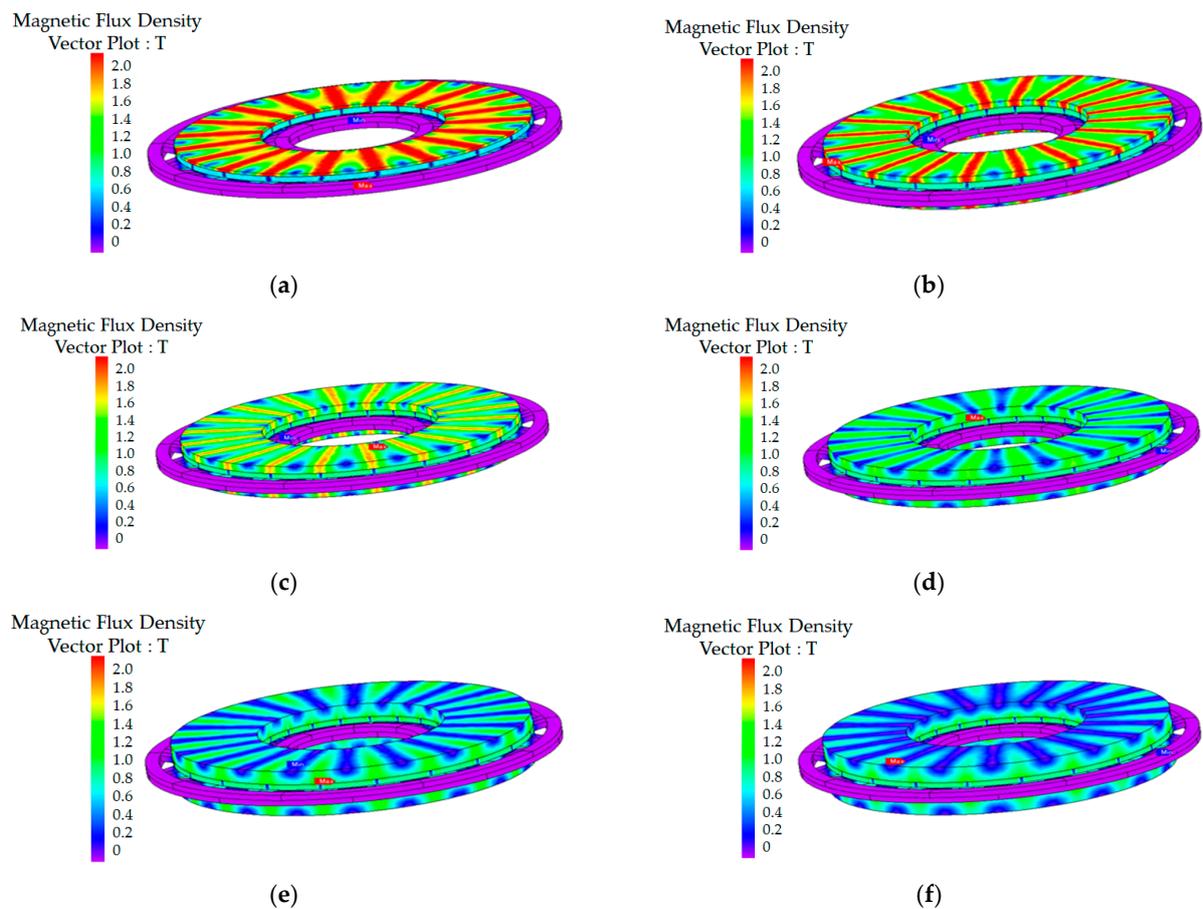
Figure 10. Core saturation analysis according to core thickness: (**a**) core thickness 1 mm, (**b**) core thickness 2 mm, (**c**) core thickness 3 mm, (**d**) core thickness 4 mm, (**e**) core thickness 5 mm, and (**f**) core thickness 6 mm.

3.5. ASFPMSM Optimal Pole Slot Combination Analysis

Based on the above analysis, it was confirmed that the back EMF of the ASFPMSM was significantly lower than that of the target model. As a result of analyzing the reasons, the motor of the ASFPMSM generally adopts a 2:3 structure or a 4:3 structure of pole number and slot number combination to use the concentrated winding to reduce the bulk of end turns. Furthermore, multi-pole and multi-slot combinations are applied to the motor to make the back yoke of the core thinner. Therefore, it is essential to analyze the combination of poles and the number of slots. The analysis of the number of poles and the number of slot combinations were performed based on the proposed model explained above, as shown in Table 3 and Figure 11.

Table 3. Analysis of poles/slots combination (2:3 structure).

Poles/Slots	No-Load Phase Back EMF	Number of Serial Turns	Magnet Volume
24p/36s	14.87 V_{rms}	48 Turn	19,739 mm^3
28p/42s	16.62 V_{rms}	56 Turn	19,739 mm^3
32p/48s	9.11 V_{rms}	32 Turn	19,739 mm^3
36p/54s	7.74 V_{rms}	36 Turn	19,739 mm^3
48p/72s	5.93 V_{rms}	48 Turn	19,739 mm^3
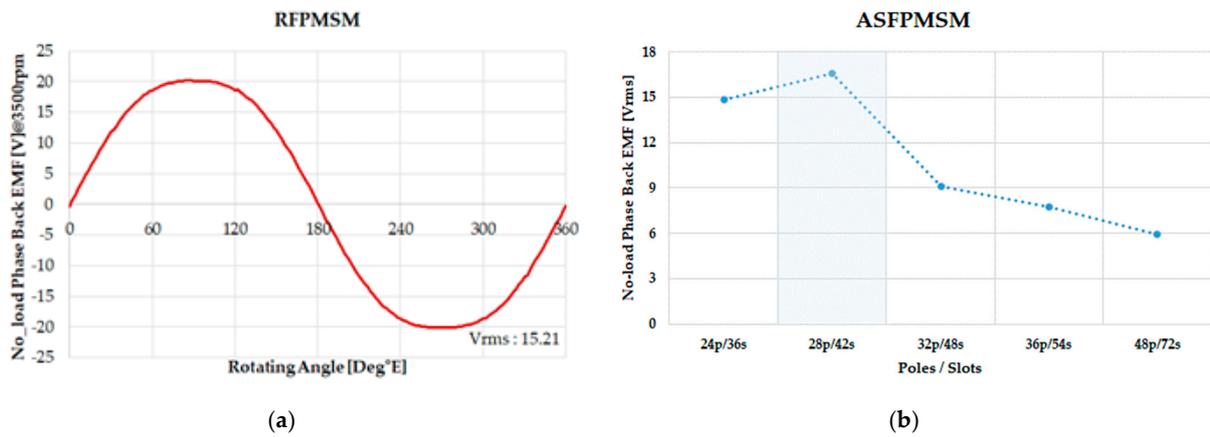
Figure 11. Comparative analysis of target RFPMSM and ASFPMSM pole/slot combination. (**a**) RFPMSM No load phase Back EMF, (**b**) ASFPMSM No load phase Back EMF according to Poles/Slots Combinations.

In cases of the block coil models, it is difficult to analyze the models while keeping the same number of turns in series per pole because there is no slot, and the area of the block on which the coil is wound varies according to the number of slots. Therefore, the size of the winding used in the target model was used according to the number of slots, and the number of windings according to the number of slots was used, as shown in Figure 12. Therefore, when the 0.85 mm winding is used, it is advantageous to minimize the gap by applying the (c) and (d) pole/slot combination in Figure 12.
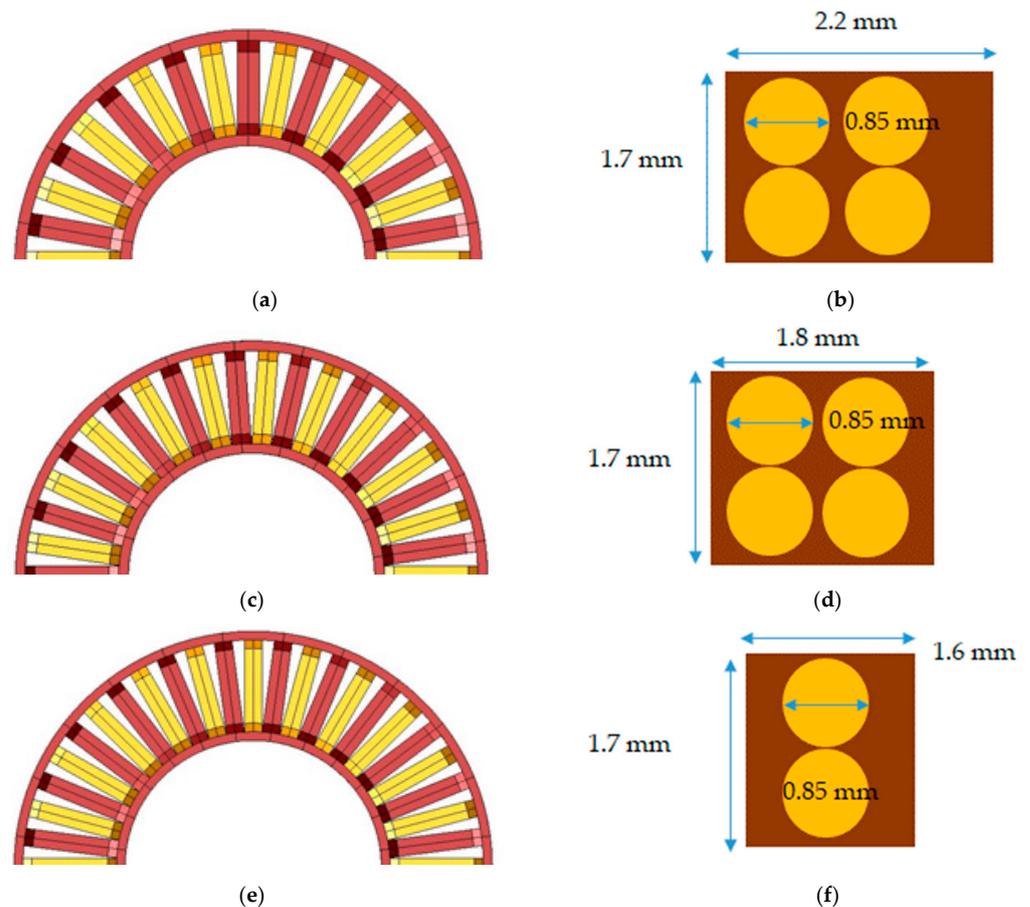
Figure 12. Coil area by pole/slot combination: (**a**) 24p/36s coil shape, (**b**) 24p/36s coil area, (**c**) 28p/42s coil shape, (**d**) 28p/42s coil area, (**e**) 32p/48s coil shape, and (**f**) 32p/48s coil area.

However, in the case of 28 poles/42 slots, there are spaces between the winding and the outline of the block when 0.85 mm thickness winding is used, as shown in Figure 13. Therefore, 0.9 mm thickness winding was checked as an optimistic design. Then, 0.9 mm thickness was shown to deliver 12% more current with the same current density (Table 4). Finally, the final model of the ASFPMSM of 28p/42s was selected based on the previously analyzed optimal design and used to comparatively analyze the performance of the existing RFPMSM load.
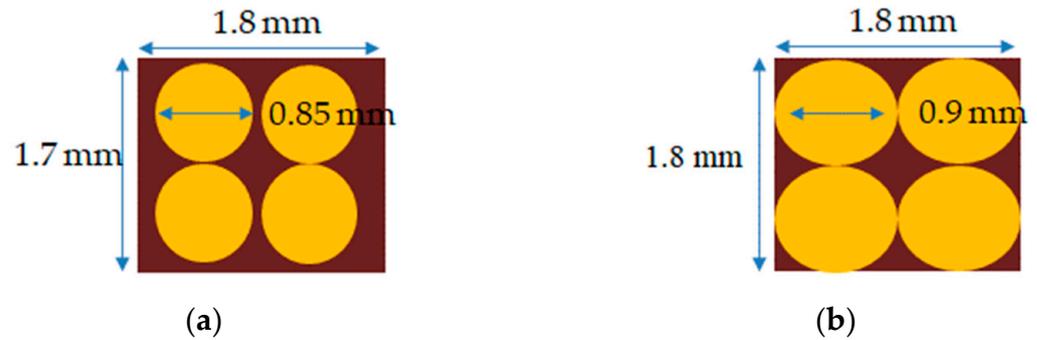

Figure 13. Coil empty space comparison: (**a**) 0.85 m, (**b**) 0.9 mm.

Table 4. Current density comparison.

Parameter	Coil 0.85	Coil 0.9	Unit
Current	5.1	5.7	A_{rms}
Coil Diameter	0.85	0.9	mm
Coil Area	0.57	0.64	mm^2
Current Density	8.98	8.98	A/mm^2

4. Optimal Designed Model Comparison Analysis

In this chapter, the final ASFPMSM model was proposed based on the above optimum design and analysis, and this was compared and analyzed with the target model, as shown in Figure 14.
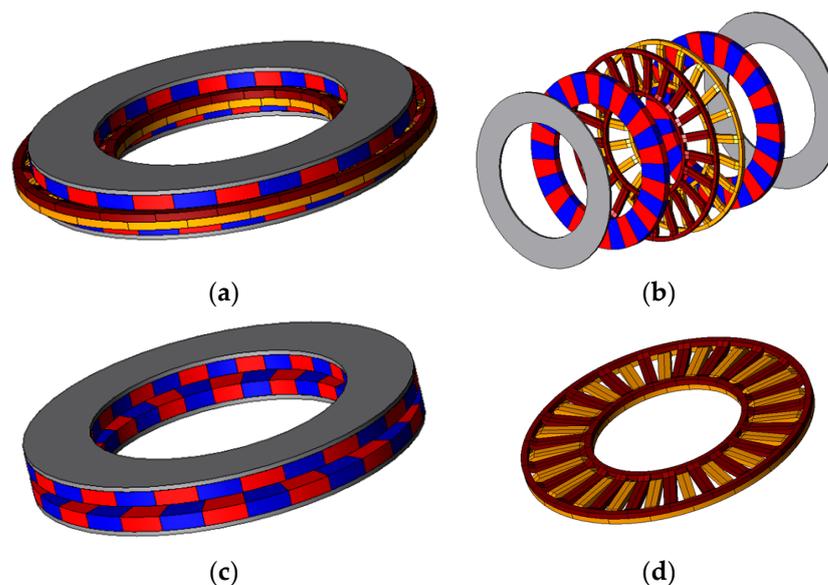

Figure 14. (**a**) Optimal design analysis model; (**b**) optimal design model exploded view; (**c**) optimally designed rotor shape; (**d**) optimally designed block coil shape.

The optimal model was proposed with the same stacking length as the target model RFPMSM with a core thickness of 2 mm, a magnet thickness of 3.3 mm, a coil thickness of 1.8 mm, and an air gap length of 0.3 mm, as shown in Table 5. More details are presented in Table 6.

Table 5. Specification of optimally designed ASFPMSM.

Parameter	Value (mm)
Rotor Outer Diameter	52.2
Rotor Inner Diameter	44.8
Magnet Length	7.4
Air Gap	0.3
Motor Stack Length	13
Magnet Thickness	3.3

Table 6. Materials of optimally designed ASFPMSM.

	Parameter	Value	Unit
Performance	Poles/Slots	28/42	-
	Rated Speed	3500	RPM
	DC Link	48	V
Winding	Material	Copper	-
	Diameter	0.9	mm
	Series Turns Per Phase	56	Turns
	Phase Resistance	0.032	Ω
Magnet	Material	N42SH	-
	B_r	1.33	T
	H_c	1592	KA/m

For comparative analysis, the no-load back EMF of the target model and the no-load back EMF of the ASFPMSM are shown in the Figure 15, and both were analyzed at the rated speed of 3500 Rpm.
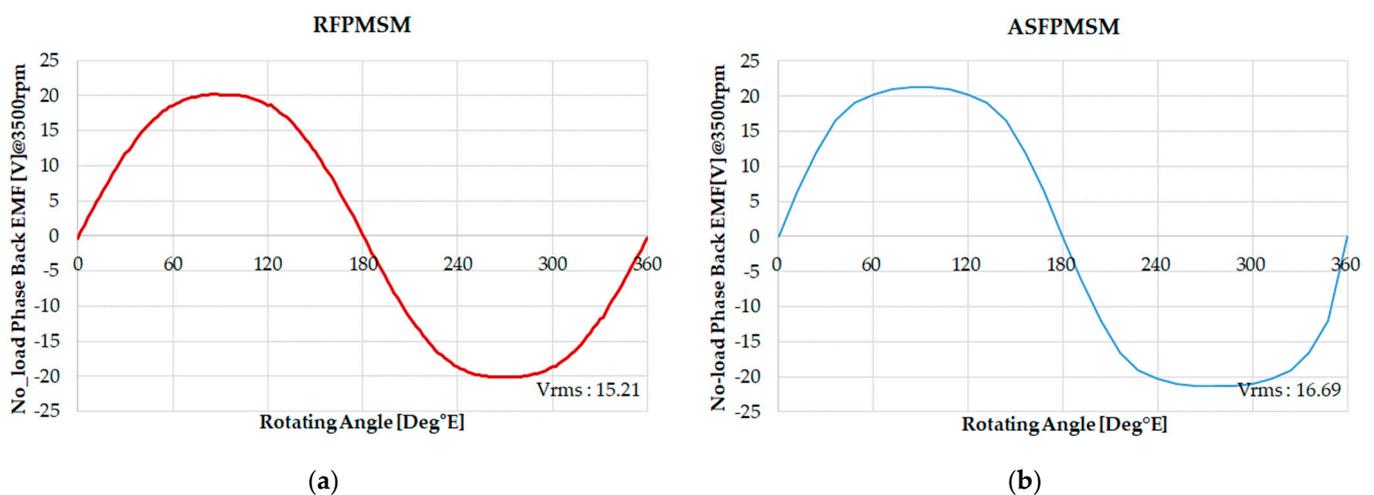

Figure 15. No load phase back EMF comparison: (**a**) no load phase back EMF of RFPMSM; (**b**) no-load phase back EMF of ASFPMSM.

As shown in Figure 15, Table 7 it was confirmed that the back EMF of the proposed model is 10% larger than that of the target model. It is validated that the performance of the proposed model is 10% higher than that of the target model at the same current density.

Table 7. Performance and materials of optimally designed ASFPMSM.

Parameter	RFPMSM	ASFPMSM	Unit
RPM	3500		r/min
DC Link	48		V
Current Density	8.98	8.98	A/mm^2
Torque	0.55	0.63	N·m
Input	226.2	235.4	W
Copper Loss	11.1	4.48	W
Iron Core Loss	12.5	0.5	W
Output	202.0	230.4	W
Efficiency	89.6	97.9	%

From load torque comparison, as shown in Figure 16, the torque of the proposed model is 20% higher than that of the target model. It was confirmed that the output power and the efficiency increased by 15% and 8.3%, respectively. In addition, it can be seen that the iron loss is very low because only iron loss from the rotor remains at no back yoke of the stator structure. Therefore, it is possible to reduce the total iron loss significantly. In the case of an axial flux motor, it is possible to reduce the surface magnetic flux density per pole by using a multi-pole structure to increase the output density in a thin structure, and design a thin rotor back yoke. However, as the back yoke becomes thinner, the rotor back yoke is saturated, and torque ripple may occur.
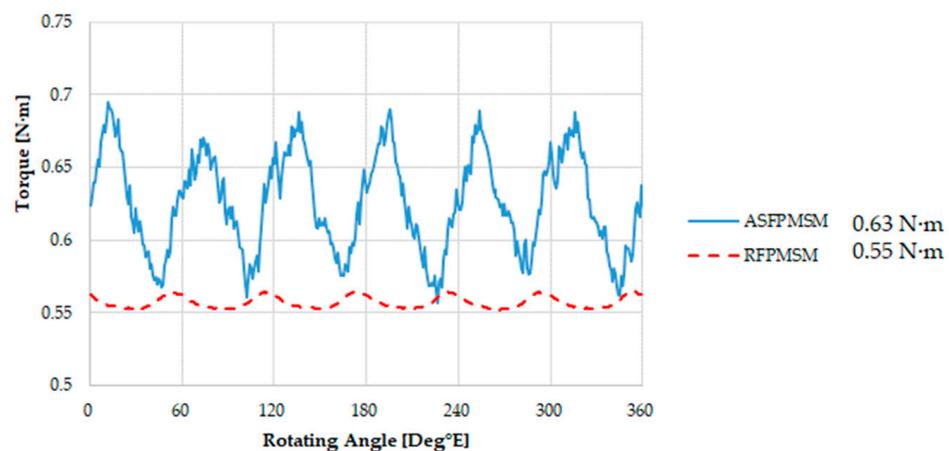
Figure 16. Load torque comparison between RFPMSM and ASFPMSM.

In the case of an axial flux motor, the main requirements are small size, lightweight, high torque density, and high power density. Therefore, torque ripple is not a main characteristic. Vibration and noise caused by torque ripple are commonly buried in external noise or other structural device noise in the applications. Even considering that the current torque ripple is 10% to 20%, it is not a high level, and there is no problem with the motor performance.

To verify the validity of the design, the magnetic flux line and magnetic flux density saturation of ASFPMSM were checked via FEA as shown in Figures 17 and 18.
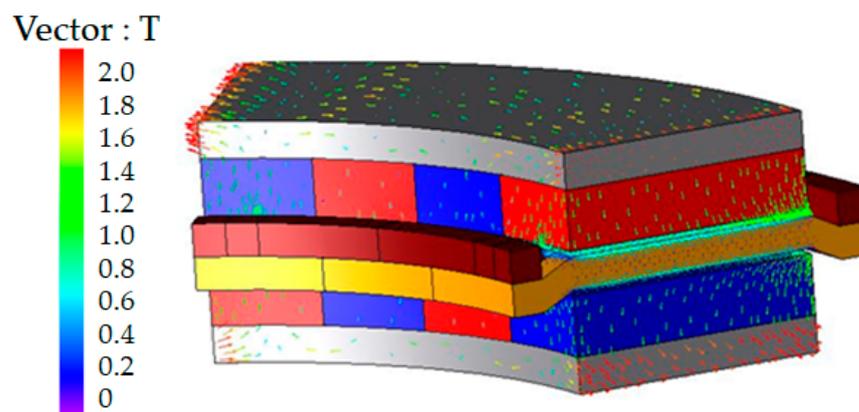
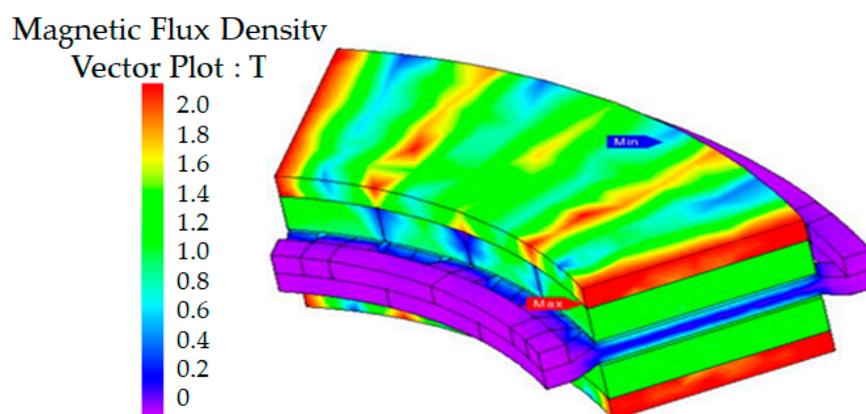**Figure 17.** Vector plot of optimally designed ASFPMSM.

Figure 18. The magnetic flux density of optimally designed ASFPMSM.

As a result of analyzing the vector diagram in Figure 17, it is confirmed that magnetic flux is formed as a closed-loop without a leakage flux problem. In addition, it is also confirmed that there was no problem with the saturation of the core at the rating power. Therefore, it was confirmed that the torque density and output power density were improved compared to the same size of the target model at the rated 3500 RPM.

5. Conclusions

In this paper, the high torque density of ASFPMSM using 3D printing technology for collaborative robots was proposed to replace the RFPMSM used in collaborative robot joints. For accurate performance comparison, the same inner diameter, outer diameter size, volume, winding size, and current density as the target model were used. The back EMF of the ASFPMSM may be smaller compared to the RFPMSM because the block coil increases the airgap. Therefore, it was necessary to analyze the design parameters to increase the performance while minimizing the leakage flux. The block winding thickness, and the total amount of magnet and pole/slot combinations were considered for optimization design. Then, the model with a core thickness of 2 mm, a magnet thickness of 3.3 mm, a coil thickness of 1.8 mm, and an air gap length of 0.3 mm was proposed. The model's 12% higher torque, 15% higher output power, and 8.3% higher efficiency than that of the RFPMSM were proved via FEA.

Author Contributions: Conceptualization, W.-H.K.; methodology, D.-Y.S.; software, D.-Y.S.; validation, D.-Y.S.; formal analysis, D.-Y.S.; investigation, D.-Y.S.; resources, D.-Y.S.; data curation, D.-Y.S. and K.-B.L.; writing—original draft preparation, D.-Y.S. and K.-B.L.; visualization, D.-Y.S., M.-J.J.; supervision, W.-H.K. and K.-D.L. All authors have read and agreed to the published version of the manuscript.

Institutional Review Board Statement: Not applicable.

Informed Consent Statement: Not applicable.

Data Availability Statement: Not applicable.

Conflicts of Interest: The authors declare no conflict of interest.

References

1. Wu, S.-H.; Hong, X.-S. Integrating Computer Vision and Natural Language Instruction for Collaborative Robot Human-Robot Interaction. In Proceedings of the 2020 International Automatic Control Conference (CACS), Hsinchu, Taiwan, 4–7 November 2020; pp. 1–5. [CrossRef]
2. Gieras, J.F.; Wang, R.-J.; Kamper, M.J. *Axial Flux Permanent Magnet Brushless Machines*; Springer Science Business Media B. V.: Berlin, Germany, 2008. [CrossRef]
3. Hanselman, D. *Brushless Motors: Magnetic Design Performance and Control*; E-Man Press LLC: Amsterdam, NY, USA, 2012.
4. Messina, G.; De Bella, E.T.; Morici, L. HTS Axial Flux Permanent Magnets Electrical Machine Prototype: Design and Test Results. *IEEE Trans. Appl. Supercond.* **2019**, *29*, 1–5. [CrossRef]
5. Andriollo, M.; Bettanini, G.; Tortella, A. Design procedure of a small-size axial flux motor with Halbach-type permanent magnet rotor and SMC cores. In Proceedings of the 2013 International Electric Machines & Drives Conference, Chicago, IL, USA, 12–15 May 2013; pp. 775–780. [CrossRef]
6. Profumo, F.; Zhang, Z.; Tenconi, A. Axial flux machines drives: A new viable solution for electric cars. *IEEE Trans. Ind. Electron.* **2002**, *44*, 39–45. [CrossRef]
7. Polat, M.; Yildiz, A.; Akinci, R. Performance Analysis and Reduction of Torque Ripple of Axial Flux Permanent Magnet Synchronous Motor Manufactured for Electric Vehicles. *IEEE Trans. Magn.* **2021**, *57*, 1–9. [CrossRef]
8. Ueda, Y.; Takahashi, H. Cogging Torque Reduction on Transverse-Flux Motor with Multilevel Skew Configuration of Toothed Cores. *IEEE Trans. Magn.* **2019**, *55*, 1–5. [CrossRef]
9. Jia, L.; Lin, M.; Le, W.; Li, N.; Kong, Y. Dual-Skew Magnet for Cogging Torque Minimization of Axial Flux PMSM With Segmented Stator. *IEEE Trans. Magn.* **2020**, *56*, 1–6. [CrossRef]
10. Polat, M.; Akinci, R. Design and analysis of axial flux double rotor permanent magnet synchronous motor for electric vehicles. *Fırat Univ. J. Eng. Sci.* **2020**, *32*, 345–358.
11. Aydin, M.; Gulec, M.; Demir, Y. Design and validation of a 24-pole coreless axial flux permanent magnet motor for a solar powered vehicle. In Proceedings of the XXII International Conference on Electrical Machines (ICEM), Lausanne, Switzerland, 4–7 September 2016.
12. Aydin, M.; Gulec, M. Reduction of Cogging Torque in Double-Rotor Axial-Flux Permanent-Magnet Disk Motors: A Review of Cost-Effective Magnet-Skewing Techniques with Experimental Verification. *IEEE Trans. Ind. Electron.* **2013**, *61*, 5025–5034. [CrossRef]
13. Neethu, S.; Nikam, S.P.; Singh, S. High-speed coreless axial-flux permanent-magnet motor with printed circuit board winding. *IEEE Trans.* **2019**, *55*, 1954–1962.
14. Wang, X.; Li, C.; Lou, F. Geometry Optimize of Printed Circuit Board Stator Winding in Coreless Axial Field Permanent Magnet Motor. In Proceedings of the IEEE Vehicle Power and Propulsion Conference (VPPC), Hangzhou, China, 17–20 October 2016; pp. 1–6. [CrossRef]
15. Jang-Young, C.; Sung-Ho, L.; Kyoung-Jin, K.; Seok-Myeong, J. Improved analytical model for electromagnetic analysis of axial flux machines with double-sided permanent magnet rotor and coreless stator windings. *IEEE Trans. Magnet.* **2011**, *47*, 2760–2763.
16. Gonzalez-Parada, A.; Trillaud, F.; Guzman-Cabrera, R.; Abatal, M. Torque Ripple Reduction in an Axial Flux High Temperature Superconducting Motor. *IEEE Trans. Appl. Supercond.* **2014**, *25*, 1–5. [CrossRef]
17. Bruzinga, G.R.; Filho, A.J.S.; Pelizari, A. Analysis and Design of 3 kW Axial Flux Permanent Magnet Synchronous Motor for Electric Car. *IEEE Lat. Am. Trans.* **2022**, *20*, 855–863. [CrossRef]
18. Zhao, F.; Kim, M.-S.; Kwon, B.-I.; Baek, J.-H. A Small Axial-Flux Vernier Machine with Ring-Type Magnets for the Auto-Focusing Lens Drive System. *IEEE Trans. Magn.* **2016**, *52*, 1–4. [CrossRef]